Geophys. J. Int. (1992) **110,** 180–190

Polarization properties of near-field waves in homogeneous isotropic and anisotropic media: numerical modelling

Václav Vavryčuk

Geophysical Institute, Czechoslovak Academy of Sciences, Boční II/1401, 141 31 Praha 4, Czechoslovakia

Accepted 1992 January 30. Received 1992 January 14; in original form 1991 June 24

SUMMARY

The paper deals with the polarization properties of complete body waves propagating in elastic, homogeneous, unbounded, isotropic and anisotropic media. The waves excited by a point dipole source and by a line dipole source in an isotropic medium are computed by the numerical integration of Green's function. The waves excited by a line dipole source in an anisotropic medium are modelled by the finite-difference method.

It is shown that complete radiation patterns of *P*- and *S*-waves of the dipole source in isotropic as well as anisotropic media do not generally have nodal lines, and that *P*- and *S*-waves are not generally polarized linearly, but quasi-elliptically. The degree of ellipticity decreases with increasing ratio r/λ and depends on the azimuth. A significant value of ellipticity was observed in the vicinity of the far-field nodal lines even for ratios $r/\lambda \approx 10$ and more. For an anisotropic medium in the vicinity of the source a difference was detected between the predominant polarization direction of complete waves and the far-field polarization direction.

Key words: anisotropic medium, finite-difference method, near-field waves, polarization.

1 INTRODUCTION

The object of this paper is the detailed study of the polarization properties of elastic waves in homogeneous, unbounded, isotropic and anisotropic media. Attention is focused on the polarization properties of the *near-field* waves in these media.

The computation of complete body waves in homogeneous *isotropic* media does not pose any special problems because an analytical form of Green's function exists for such a medium. Since no analytical solutions are as yet available for complete body waves in general *anisotropic* media, these waves are still only modelled numerically (Fryer & Frazer 1984; Mandal & Mitchell 1986; Taylor 1987; Mallick & Frazer 1990; Mandal & Toksöz 1990; Tsingas, Vafidis & Kanasewich 1990; Tsvankin & Chesnokov 1990). Most of the studies in which complete wavefields are modelled do not, however, analyse the polarization properties of waves. On the contrary, wave polarization studies (Keith & Crampin 1977; Crampin, Stephen & McGonigle 1982) do not consider the contributions of the near-field waves, and remain at the level of interpretation of far-field wave polarization. For such interpretations it would be sufficient to apply the much more effective ray approach to computing waves in anisotropic media (Gajewski & Pšenčík 1987, 1990). An exception is the paper by Tsvankin & Chesnokov (1990), who point out the significance of the near-field terms, especially in the vicinity of the nodal lines of far-field waves, and refer to the complicated polarization properties of the complete wavefield in an anisotropic medium.

The reason for the lack of papers with a more precise analysis of the polarization properties of the complete wavefield in anisotropic as well as in isotropic media is probably the widespread *underestimation of the near-field contributions* (e.g. Farra, Bernard & Madariaga 1986). But this attitude contradicts the present efforts to study the seismic source from the smallest possible hypocentral distance, on the one hand, and fails to consider the fact that wave polarization is very sensitive to near-field contributions, on the other.

The above-mentioned detailed analysis of the polarization properties of the complete wavefield will be made on synthetic seismograms computed for an isotropic medium by *numerical integration of Green's function,* and for an anisotropic medium by the *finite-difference method* (see e.g. Kelly *et al.* 1976; Frankel & Clayton 1986; Hong & Bond 1986; Levander 1988; Daudt *et al.* 1989; Tsingas *et al.* 1990).

Downloaded from http://gji.oxfordjournals.org/ at Astronomical Institue CAS on August 4, 2015

2 FINITE-DIFFERENCE METHOD

Finite-difference equation for a homogeneous anisotropic medium

In the following we will confine ourselves to the solution of the 2-D problem, i.e. we will simplify the problem so that the resulting displacement field $u_i(x_j, t)$ depends only on two space coordinates and time $u_i = u_i(x, y, t)$, $i = 1, 2, 3$.

In converting the derivatives in the elastodynamic equation (Aki & Richards 1980, formula 2.17) into finite differences, we will apply the standard *centred-difference formulae of second-order accuracy* (Aki & Richard II 1980, p. 775, Box 13.4) and we will use the so-called *explicit scheme*. Thus the system of finite-difference equations reads

$$u_i(t + \Delta t) = \Delta t^2/\rho[f_i + c_{ijkl}\,\Delta^2 u_k/\Delta x_j\,\Delta x_l] - 2u_i(t) + u_i(t - \Delta t), \quad i = 1, 2, 3, \tag{1}$$

holding for

$j = l = 1$:

$$\Delta^2 u_k/\Delta x_j\,\Delta x_l = \Delta^2 u_k/\Delta x^2 = [u_k(x + \Delta x, y) - 2u_k(x, y) + u_k(x - \Delta x, y)]/\Delta x^2,$$

$j = l = 2$:

$$\Delta^2 u_k/\Delta x_j\,\Delta x_l = \Delta^2 u_k/\Delta y^2 = [u_k(x, y + \Delta y) - 2u_k(x, y) + u_k(x, y - \Delta y)]/\Delta y^2,$$

$j = 1$, $l = 2$ or $j = 2$, $l = 1$:

$$\Delta^2 u_k/\Delta x_j\,\Delta x_l = \Delta^2 u_k/\Delta x\,\Delta y = [u_k(x + \Delta x, y + \Delta y) - u_k(x + \Delta x, y - \Delta y) - u_k(x - \Delta x, y + \Delta y) + u_k(x - \Delta x, y - \Delta y)]/4\Delta x\,\Delta y,$$

$j = 3$ or $l = 3$:

$$\Delta^2 u_k/\Delta x_j\,\Delta x_l = 0,$$

where Δt is the time step; Δx, Δy is the space step; c_{ijkl} are the components of Hooke's tensor of elastic coefficients; $u_k = u_k(x, y, t)$ are the components of the displacement vector; ρ is the density of the medium; and $f_i = f_i(x, y, t)$ are the components of the acting body force.

Stability conditions of the finite-difference scheme

A physically meaningful numerical computation presumes the *stability* of the finite-difference algorithm (Mitchell 1969, p. 34). This condition is satisfied if the inequality

$$\Delta t \le \Delta x/(v_P^2 + v_S^2)^{1/2}, \tag{2}$$

(Alterman & Lowenthal 1970, formula 75), where v_P, v_S are the velocities of P- and S-waves, is valid. In the case of an anisotropic medium v_P, v_S denote the maximum values of P- and S-wave group velocities.

A condition connected with *grid dispersion* is added to formula (2):

$$\lambda_{\min} \ge 10\,\Delta x \tag{3}$$

(Alford, Kelly & Boore 1974, fig. 4).

Satisfaction of both inequalities (2) and (3) cannot be taken strictly as a sufficient condition, but rather to the effect that the better they are satisfied, the more exact a solution we will obtain.

Boundary and initial conditions

As mentioned above, we will study the polarization properties of waves propagating through an *unbounded* medium. We will practically satisfy this condition by dealing only with the direct wave. The receiver position relative to the boundary of the finite-difference model will be chosen in such a manner that the waves reflected from this boundary will arrive at times sufficient for the separation of the direct wave.

In order to define the boundary conditions, we will specify a *rigid boundary*, i.e. for every time level we will put all the three displacement components equal to zero at the boundary points. This physically means that the boundary is subject to no deformations.

Zero displacement for times $t \le 0$ and all the grid points will be chosen as the initial conditions.

Source of waves

The source of waves will be the discrete representation of a point dipole source in the 2-D model. The source will be placed inside the model and will be identified with the coordinate origin. This source is equivalent to a *line source* in the 3-D medium with the source line perpendicular to the 2-D model grid.

The discrete representation of the line source reads

$$f_i(\mathbf{x}, t) = F_i(t)\,\delta^D(\mathbf{x}), \quad i = 1, 2, 3$$

for a *line single force*,

$$f_i(\mathbf{x}, t) = M_{ij}(t) \cdot \nabla_j\,\delta^D(\mathbf{x}), \quad i = 1, 2, 3 \tag{4}$$

for a *line dipole force*,

where $F_i(t)$ are the components of the force vector, $M_{ij}(t)$ are the components of the moment tensor, $\delta^D(\mathbf{x}) = \delta^D(x) \cdot \delta^D(y)$ is the discrete representation of the standard Dirac function (see Fig. 1), and $\nabla_j\,\delta^D(\mathbf{x})$ is the discrete representation of the Dirac function derivative (see Fig. 1).

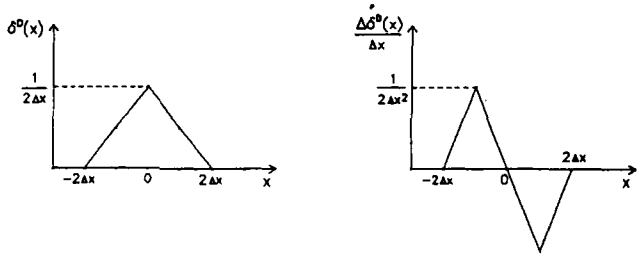

Figure 1. Discrete representation of Dirac delta function $\delta^D(x)$ and of its derivative $\Delta\,\delta^D(x)/\Delta x$. The representation is taken from Aboudi (1971), but the error in the maximum amplitude of both functions has been removed.

Downloaded from http://gji.oxfordjournals.org/ at Astronomical Institute CAS on August 4, 2015

3 ISOTROPIC MEDIUM

In the following we will deal with the properties of elastic waves excited by a point and line dipole source, and propagating in a homogeneous, isotropic, unbounded medium. An analytical form of Green's function is available for this medium (see Aki & Richards 1980, formula 4.23), and the solution of the complete wavefield can be obtained by its simple numerical integration. This computation will also be used to test the accuracy of the finite differences (FD).

3.1 Point and line sources: exact solution

Computation of the exact solution

The displacement field $u_n(x_k, t)$ excited by a dipole source is given by the *representation theorem* (Aki & Richards 1980, formula 3.19), which takes the following form for a *point source*,

$$u_n(x_k, t) = \int_0^\infty M_{ij}(\tau) G_{ni,j}(x_k, t; \xi_k, \tau)\, d\tau,$$
$$n = 1, 2, 3, \tag{5}$$

and for a *line source* (identical with axis z),

$$u_n(x_k, t) = \int_{-\infty}^{\infty} \int_0^\infty m_{ij}(\xi_3, \tau) G_{ni,j}(x_k, t; \xi_k, \tau)\, d\xi_3\, d\tau,$$
$$n = 1, 2, 3, \tag{6}$$

where $M_{ij}(t)$ is the moment tensor, $m_{ij}(\xi_3, t)$ is the linear moment-density tensor, $G_{ni,j}(x_k, t; \xi_k, \tau)$ is the spatial derivative of Green's function for a homogeneous, isotropic, unbounded medium (see Aki & Richards 1980, formula 4.29), x_j are the components of the position vector of the receiver, and ξ_j are the components of the position vector of the source.

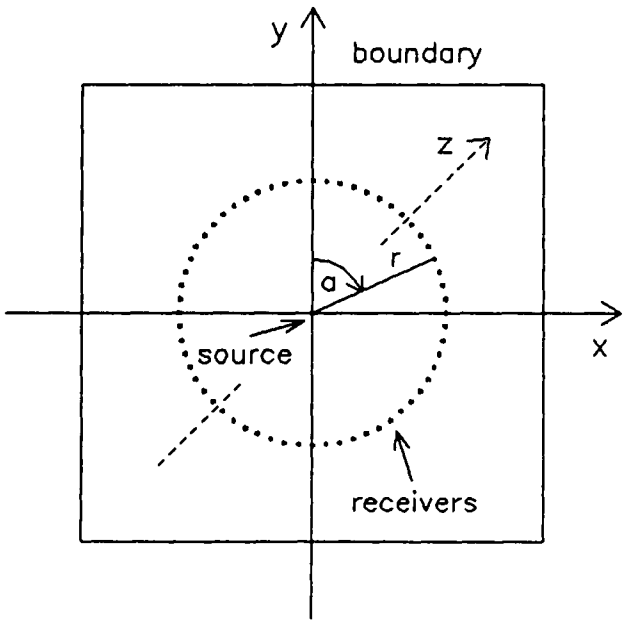

Figure 2. Diagram of source and receiver positions. r is the distance of the receivers from the source, a is the azimuth of a receiver.

Formulae (5) and (6) make it possible to compute the wavefield excited by a source situated in a homogeneous, isotropic, unbounded medium. The integrals in (5) and (6) can be easily determined numerically and, moreover, the required accuracy of the resulting solution can be guaranteed by the choice of a sufficiently small integration step. Therefore, the solution obtained from (5) and (6) will be referred to as the *exact solution* in contrast to the FD solution which will be called the *approximate solution*.

Configuration of experiment and medium model

The point source is placed in the origin of coordinates, the line source is identical with axis z (see Fig. 2). The receivers lie in the plane $z = 0$ and are regularly distributed around the source (see Fig. 2). The mutual distance of the receivers in azimuth a amounts to 6°.

The velocities of P- and S-waves are taken to be $v_P = 5.60\,\mathrm{km\,s^{-1}}$, $v_S = v_P/\sqrt{3}$, and, consequently, Hooke's matrix, normalized by the density of the medium, then has the form (the values are given in units of $10^6\,\mathrm{m^2\,s^{-2}}$)

$$c_{ij} = \begin{pmatrix} 31.360 & 10.453 & 10.453 & 0.000 & 0.000 & 0.000 \\ & 31.360 & 10.453 & 0.000 & 0.000 & 0.000 \\ & & 31.360 & 0.000 & 0.000 & 0.000 \\ & & & 10.453 & 0.000 & 0.000 \\ & & & & 10.453 & 0.000 \\ & & & & & 10.453 \end{pmatrix}.$$

In the following, by Hooke's matrix we will always understand a matrix normalized by the density of the medium.

The tensors $M_{ij}(t)$ and $m_{ij}(\xi_3, t)$ have a coincident form, and are chosen either as

$$M_{ij}(t) = m_{ij}(t) = \begin{pmatrix} 0 & 1 & 0 \\ 1 & 0 & 0 \\ 0 & 1 & 0 \end{pmatrix} \cdot g(t), \tag{7}$$

or as

$$M_{ij}(t) = m_{ij}(t) = \begin{pmatrix} 0 & 1 & 0 \\ 1 & 0 & 0 \\ 0 & 0 & 0 \end{pmatrix} \cdot g(t). \tag{8}$$

The source-time function $g(t)$ has the form

$$g(t) = \int_0^t g_1(\tau)\, d\tau,$$
$$g_1(t) = \begin{cases} \sin^4(2\pi f t) & \text{for } t \in \langle 0, 2/f \rangle, \\ 0 & \text{for } t \in (2/f, \infty). \end{cases} \tag{9}$$

The source-time function $g(t)$ has been chosen so that the wave has the form of a one-sided pulse for the point source in the far-field approximation and thus is a good approximation of the source-time function of simple earthquake events. The power 4 is used to get a rapid decrease of the high-frequency part of the spectrum of the propagating pulse. The parameter f specifies the pulse width and, consequently, the predominant wavelength λ of the radiated wave; f was selected alternatively as $f = 0.6$ Hz and $f = 1.0$ Hz.

Downloaded from http://gji.oxfordjournals.org/ at Astronomical Institute CAS on August 4, 2015

Formula (7) describes a general dipole source, while formula (8) describes a double-couple source. In seismology, the double-couple is the most frequently used source, but in the case of a line source, which is placed in an isotropic medium as described above, the double-couple does not generate the displacement component $u_3(x_k, t)$. For this reason, in some analyses we also use source (7).

Waveforms and radiation patterns

Fig. 3 shows a comparison of the waveforms excited by a point and a line source. The tensors M_{ij} and m_{ij} were computed using formulae (7) and (9) for $f = 0.6$ Hz. The waveforms are shown in the system of axes L-Q-T, which is defined in the following way. Axis L is oriented along the source–receiver line, axis Q is parallel to axis z and axis T lies in the x–y plane. All three axes L, Q, T are mutually perpendicular.

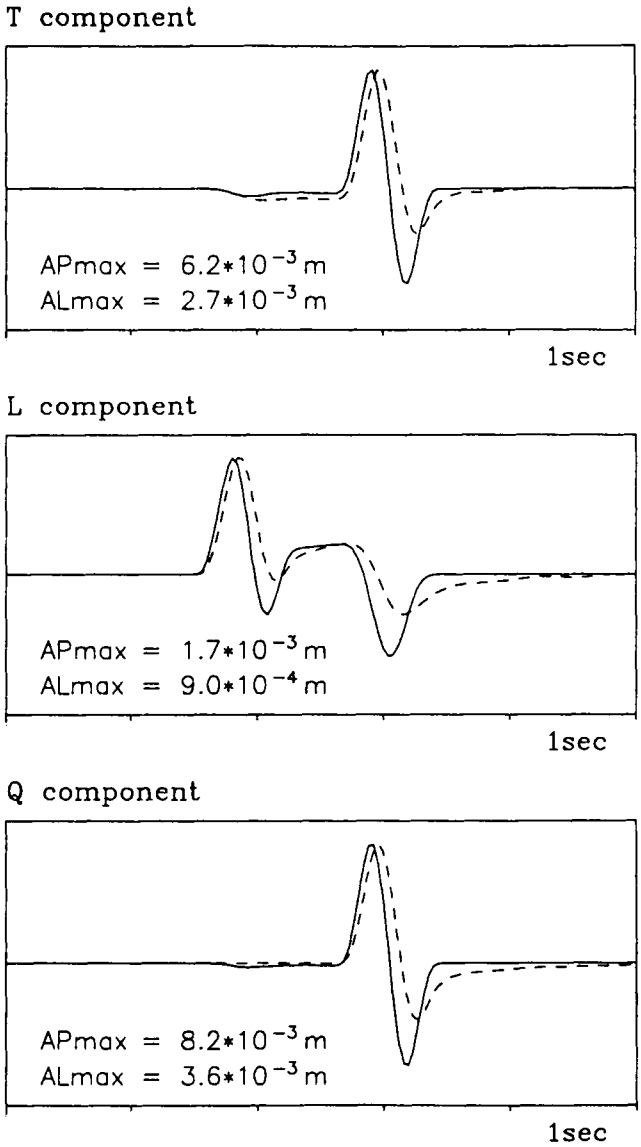

Figure 3. Velocity records of waves excited by a point and a line source. For the receiver at the position $\mathbf{x} = (x, y, 0)$, where $x = r \sin(a)$, $y = r \cos(a)$, $a = 24°$, $r = 8.6$ km ($r/\lambda_P = 0.9$, $r/\lambda_S = 1.6$), the normalized velocity records are depicted in the L-Q-T coordinate system. The waves are excited by a point source (full line, maximum amplitude AP_{max}) and by a line source (dashed line, maximum amplitude AL_{max}).

The waveforms for the point and the line source are similar, but, nevertheless, they do exhibit some differences. The waves excited by the line source have suppressed overshoots and the waves die away more slowly. The waves of the line source display a slight time delay relative to the waves excited by the point source.

By *radiation patterns* we will understand the vector sum of maximum amplitudes measured in components of velocity records for a particular wavegroup for receivers at a given distance r from the source.

Figs 4(a) and (b) show the radiation patterns of P- and S-waves of the point and the line source for the component lying in the x–y plane $[v = (\dot{u}_x^2 + \dot{u}_y^2)^{1/2}]$ and for the component perpendicular to it ($w = |\dot{u}_z|$). Tensors M_{ij} and m_{ij} were computed according to (7) and (9) for $f = 1.0$ Hz.

Comparing Figs 4(a) and (b) we can draw the following conclusions:

(1) *For component* v the complete radiation patterns of P- and S-waves for the point and the line source are very similar. They have the quatrefoil form well-known from the far-field radiation patterns of a point double-couple source (see Aki & Richards 1980, pp. 82, 83).

(2) This form, however, is frequency and distance dependent, or more exactly, it depends on ratio r/λ, where λ is the predominant wavelength of the radiated wave and r is the distance, at which the complete radiation pattern is measured.

(3) As opposed to far-field radiation patterns, there are no directions in which the source does not radiate, i.e. *nodal lines do not exist.* However, the amplitudes of waves radiated in the directions of the far-field nodal lines very quickly tend to zero with increasing distance.

(4) *For component* w the radiation patterns of S-waves for the point and the line source are very similar, but in the case of P-waves they distinctly differ. This is due to the radiation pattern of P-waves for the line source being identically zero. The reason is the separation of the system of equations of motion into equations that solve the problem of P–SV waves and the equation that solves the problem of SH-waves, the latter generating no P-waves. Let us add that, in the case of a double-couple source lying in the x–y plane, the radiation patterns of P- as well as S-waves would be identically zero for component w and the point and line source.

Polarization

A comparison of the polarization properties of waves excited by a point and line source will be made for a double-couple source lying in the x–y plane (formulae 8, 9) for $f = 0.6$ Hz.

Compared with the far-field wave polarization, the polarization properties of the complete wavefield differ in an essential way. Neither P-waves nor S-waves are linearly polarized but have *quasi-elliptical polarization* (see Fig. 5). This polarization is due to the near-field waves, which are

Downloaded from http://gji.oxfordjournals.org/ at Astronomical Institute CAS on August 4, 2015

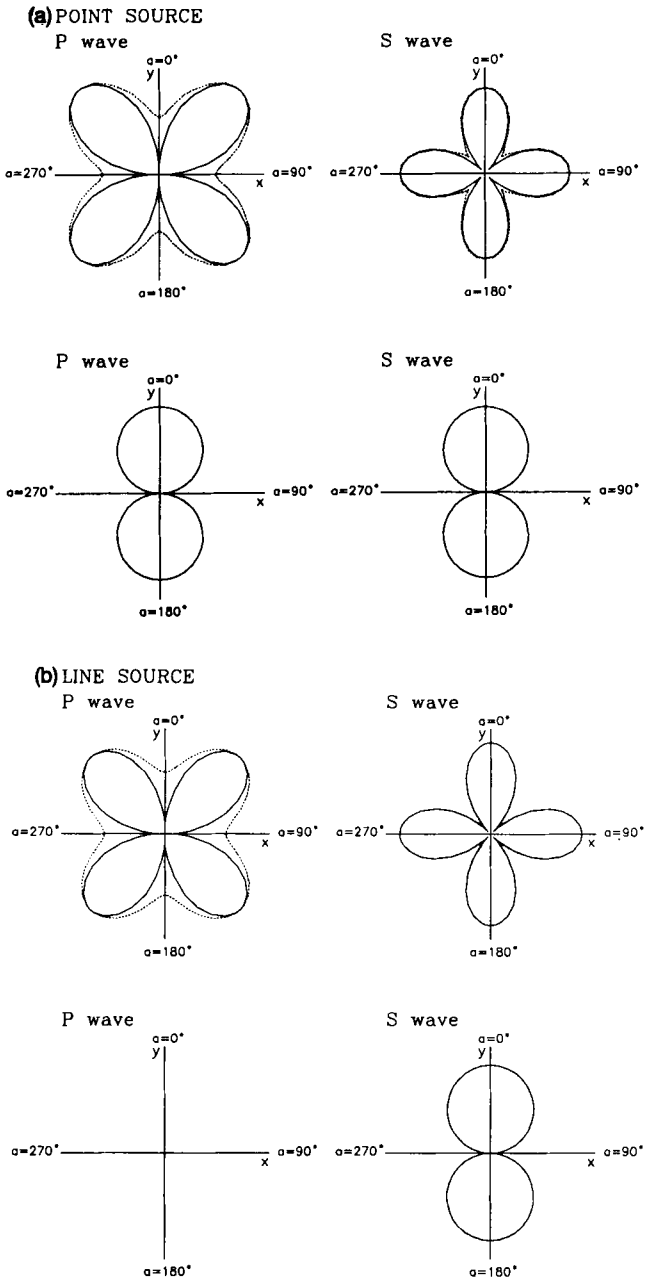

Figure 4. (a) Radiation patterns of *P*- and *S*-waves excited by a point source. The radiation patterns of *P*- and *S*-waves are shown in the x–y plane for component $v = [\dot{u}_x^2 + \dot{u}_y^2]^{1/2}$ (upper parts) and for component $w = |\dot{u}_z|$ (lower parts). The radiation patterns are measured at distances $r_1 = 2.8$ km (dotted line, $r/\lambda_P = 0.5$, $r/\lambda_S = 0.9$) and $r_2 = 16.8$ km (full line, $r/\lambda_P = 3.0$, $r/\lambda_S = 5.2$). The radiation patterns are normalized to their maximum amplitude. (b) Radiation patterns of *P*- and *S*-waves excited by a line source. For details see (a).

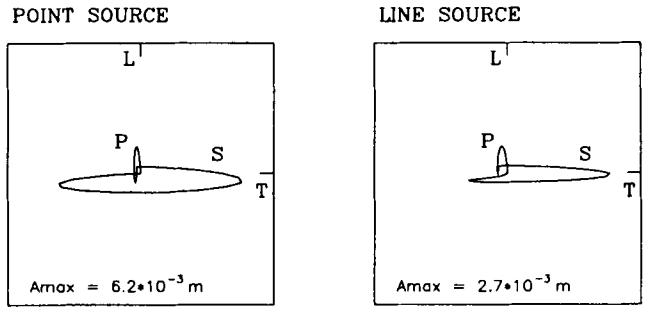

Figure 5. Polarization diagrams of velocity records of waves excited by a point and a line double-couple source. Polarization diagrams *L*-*T* are shown for the receiver with azimuth $a = 24°$ and distance $r = 8.6$ km ($r/\lambda_P = 0.9$, $r/\lambda_S = 1.6$). Component Q is identically zero for both source types. A_{max} denotes the maximum amplitude of waves displayed in the polarization diagram.

polarized in a different direction and have a different waveform than the far-field waves (see Aki & Richards 1980, formula 4.29). The result is the 'contamination' of the linearly polarized far-field *P*- and *S*-waves by near-field contributions causing the *P*-wave to have a non-zero transverse component and the *S*-wave to have a non-zero longitudinal component. This character is preserved for the velocity wavefield $\dot{u}_n(x_j, t)$ of the point as well as the line source. The difference in the polarization of waves excited by the point and the line source concerns the degree of their ellipticity.

In the following we will evaluate the degree of ellipticity of the *P*- and *S*-waves. This evaluation will serve as an estimation of the degree of 'contamination' of the far-field waves by the near-field contributions.

Let us define *ellipticity* e of the *P*-wave polarization as the ratio of the maximum amplitude of the transverse component (T) to the maximum amplitude of the longitudinal component (L), and vice versa for *S*-waves. And let us define a 'significantly contaminated far-field wave' as a wave, for which the near-field contributions produce 20 per cent ellipticity or more.

Studying *P*- and *S*-wave ellipticity for a point as well as a line double-couple source with $f = 1.0$ Hz as a function of azimuth a and ratio r/λ, we find very strong variations (see Figs 6a, b). For both types of waves and both sources we can observe a very rapid increase of ellipticity in the vicinity of the far-field nodal-line directions. With increasing r/λ the 'significantly contaminated far-field wave' is radiated in directions concentrating more and more closely to the far-field nodal-line directions, for which, strictly speaking, ellipticity is singular for all ratios r/λ. The width of the interval of directions, in which the 'significantly contaminated far-field wave' is radiated, is evaluated in Table 1 for different ratios r/λ. Table 1 shows that even for $r/\lambda = 9$ the width of the direction interval with contaminated waves amounts to almost 10 per cent of the whole interval of angles. This finding disagrees with the commonly accepted idea that near-field contributions are negligible for distances larger than λ (see Farra *et al.* 1986).

3.2 Line source: finite differences

The accuracy of the numerical solution obtained by the finite-difference method will be tested for the line dipole source situated in a homogeneous, isotropic, unbounded medium. As said before, by exact solution we will understand the solution obtained from (6), and by approximate solution we will understand the FD solution.

To check the accuracy of FD, we adopted the same configuration of the numerical experiment as in Section 3.1 (see Fig. 2). For both solutions we compared the waveforms

Downloaded from http://gji.oxfordjournals.org/ at Astronomical Institute CAS on August 4, 2015

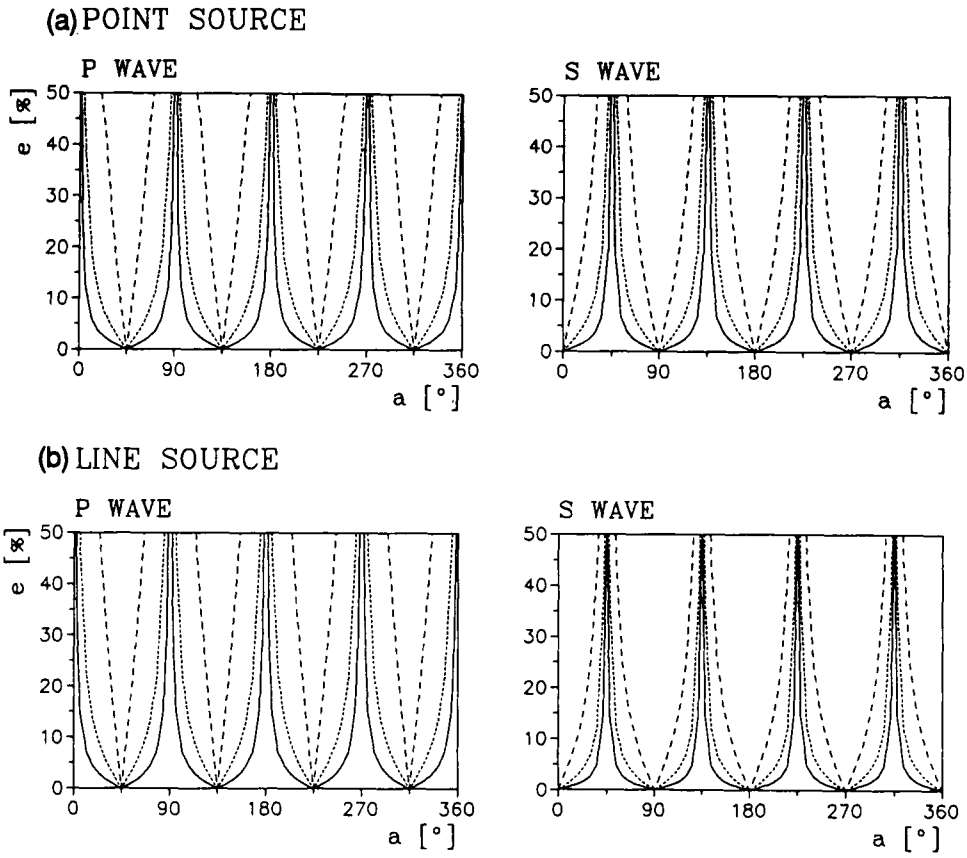

Figure 6. (a) Ellipticity of waves excited by a point source as a function of the receiver azimuth. The wave ellipticity of *P*- and *S*-waves is measured at distances $r_1 = 2.8$ km (dashed line, $r/\lambda_P = 0.5$, $r/\lambda_S = 0.9$), $r_2 = 16.8$ km (dotted line, $r/\lambda_P = 3.0$, $r/\lambda_S = 5.2$) and $r_3 = 50.4$ km (full line, $r/\lambda_P = 9.0$, $r/\lambda_S = 15.6$). The wave ellipticity has singularities and the graph was clipped at the value $e = 50$ per cent. (b) Ellipticity of waves excited by a line source as a function of the receiver azimuth. For details see (a).

Table 1. Contamination of waves by the near-field contributions—isotropic medium.

Point source				Line source			
P wave		S wave		P wave		S wave	
r/λ	c[%]	r/λ	c[%]	r/λ	c[%]	r/λ	c[%]
0.5	75	0.9	60	0.5	78	0.9	38
3.0	24	5.2	20	3.0	27	5.2	13
9.0	9	15.6	7	9.0	10	15.6	4

c denotes the interval width (in per cent) of directions in which a 'significantly contaminated far-field wave' is radiated.

of velocity field $\dot{u}_n(x_j, t)$ and the *P*- and *S*-wave radiation patterns.

Waveforms and radiation patterns

The following conclusions ensue from the comparison of the velocity waveforms for the source computed from (7) and (9) for values $f = 1.0$ Hz and $f = 0.6$ Hz (see Fig. 7):

(1) The agreement between the approximate solution and the exact one is better in both cases for *P*-waves than for *S*-waves.

(2) The agreement of the whole seismogram is better for a longer source pulse ($f = 0.6$ Hz). For $f = 1.0$ Hz the approximate solution gives an erroneous amplitude of *S*-waves and false overshoots.

In comparing the radiation patterns (see Figs 8a, b), we will arrive at analogous conclusions:

(1) The radiation pattern of *P*-waves exhibits smaller differences between the approximate solution and the exact one than the radiation pattern of *S*-waves.

(2) For $f = 0.6$ Hz the agreement in the radiation patterns of *P*- and *S*-waves can be regarded as satisfactory.

Errors of finite differences

Worse agreement in the waveforms and radiation patterns for $f = 1.0$ Hz (Fig. 7 left, Fig. 8a) is caused by grid dispersion.

Azimuthally dependent grid dispersion (see Fig. 8a) introduces *grid anisotropy*, i.e. azimuthal dependence of the wave propagation velocity. In our case this effect is weak and produces 2.4 per cent (1.2 per cent) *P*-wave and 2.8 per cent (1.4 per cent) *S*-wave velocity variations for $f = 1.0$ (0.6) Hz.

Downloaded from http://gji.oxfordjournals.org/ at Astronomical Institute CAS on August 4, 2015

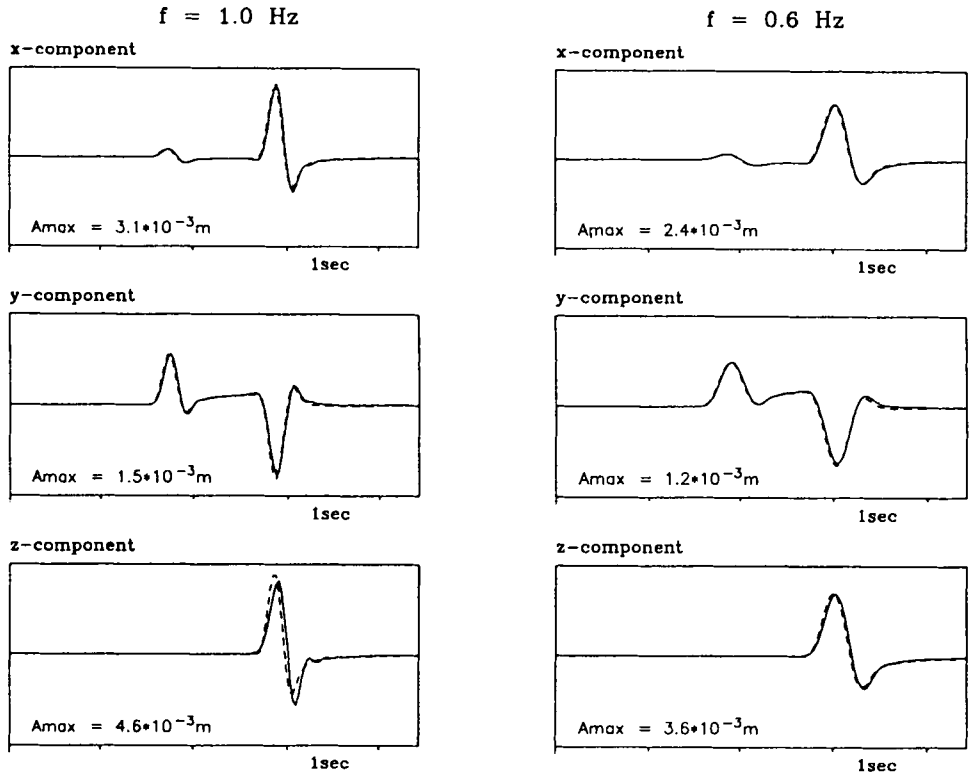

Figure 7. Velocity records of waves excited by a line source for $f = 1.0$ Hz and $f = 0.6$ Hz. A comparison of the exact solution (dashed line) and the FD solution (full line) is made for the receiver with azimuth $a = 24°$ and distance $r = 8.6$ km. A_{max} denotes the maximum amplitude of the exact solution. For a given component both solutions are displayed on the same scale. The FD parameters used are: $\Delta x = \Delta y = 0.0910$ km, $\Delta t = 0.0075$ s, size of the model 330 $\Delta x \cdot 330\ \Delta y$, number of time levels $n = 600$.

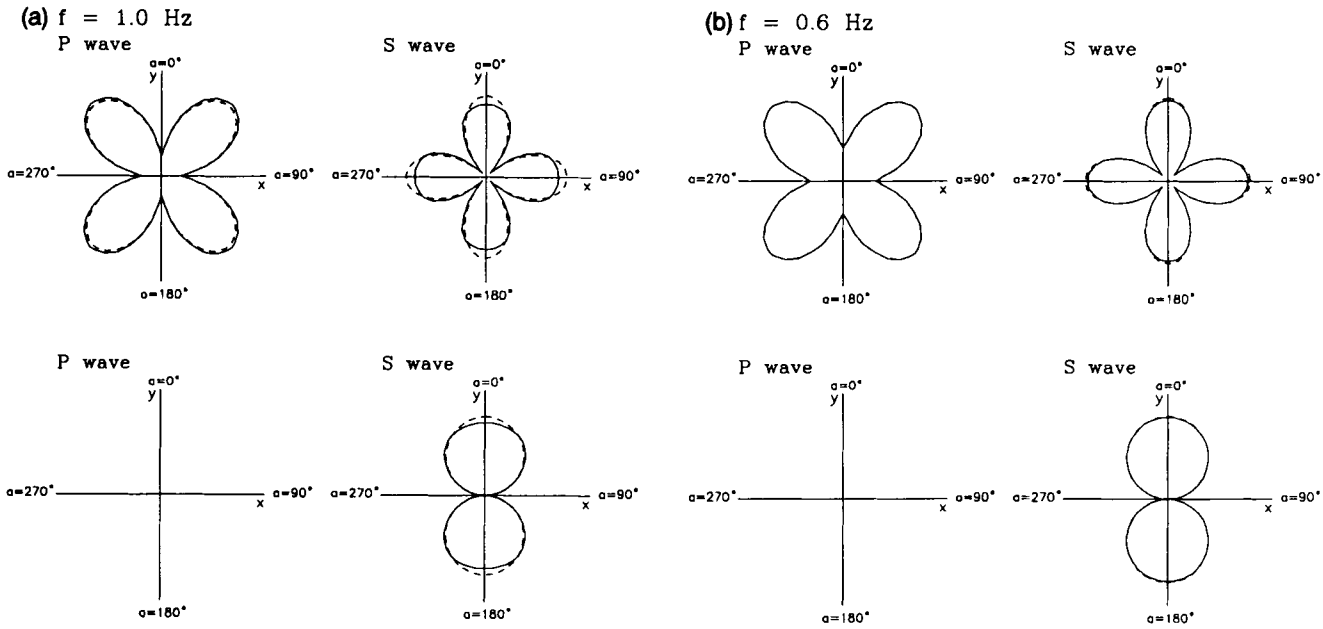

Figure 8. (a) Radiation patterns of *P*- and *S*-waves excited by a line source with $f = 1.0$ Hz. Comparison of the exact solution (dashed line) and the FD solution (full line) is made for distance $r = 8.6$ km ($r/\lambda_P = 1.5$, $r/\lambda_S = 2.7$). (b) Radiation patterns of *P*- and *S*-waves excited by a line source with $f = 0.6$ Hz. Comparison of the exact solution (dashed line) and the FD solution (full line) is made for distance $r = 8.6$ km ($r/\lambda_P = 0.9$, $r/\lambda_S = 1.6$).

Downloaded from http://gji.oxfordjournals.org/ at Astronomical Institue CAS on August 4, 2015

4 ANISOTROPIC MEDIUM

In this section we will study the behaviour of elastic waves excited by a line dipole source and propagating in a homogeneous anisotropic unbounded medium. Since an exact analytical solution is not known, we will only apply the FD method. The results of the analysis of FD accuracy made in Section 3.2 indicate that the results of FD for $f = 0.6$ Hz can be regarded as sufficiently accurate, and the question of accuracy will no longer be considered. Because of the large amount of computer time required for the FD method, we will analyse the wave properties only for one special example of anisotropy. Thus, the aim is not a detailed parametric study, but only forming an idea of wave behaviour, above all of the near-field contributions.

Configuration of experiment and medium model

The configuration of the numerical experiment is identical with that presented in Section 3.1 (see Fig. 2).

A homogeneous anisotropic medium will be defined by a normalized Hooke's matrix in the form (the values are given in units of $10^6\ m^2\ s^{-2}$)

$$c_{ij} = \begin{pmatrix} 31.360 & 6.272 & 10.453 & 0.000 & 0.000 & 0.000 \\ & 11.290 & 6.272 & 0.000 & 0.000 & 0.000 \\ & & 31.360 & 0.000 & 0.000 & 0.000 \\ & & & 6.272 & 0.000 & 0.000 \\ & & & & 10.453 & 0.000 \\ & & & & & 6.272 \end{pmatrix}.$$

The matrix describes a transversely isotropic medium with the rotation symmetry axis in the direction of axis y. Three far-field waves propagate in this medium: the P-wave and the $S2$-wave (slower S-wave), which are polarized in the x–y plane, and the $S1$-wave (faster S-wave), which is polarized in the direction parallel to axis z. Figs 9 and 10 display phase and group velocity variations for P, $S1$ and $S2$ far-field waves and the polarization angle for P and $S2$ far-field waves as a function of the receiver azimuth. In these calculations standard analytical formulae for a transversely isotropic medium in the far-field approximation have been used (see, e.g., Červený, Molotkov & Pšenčík 1977).

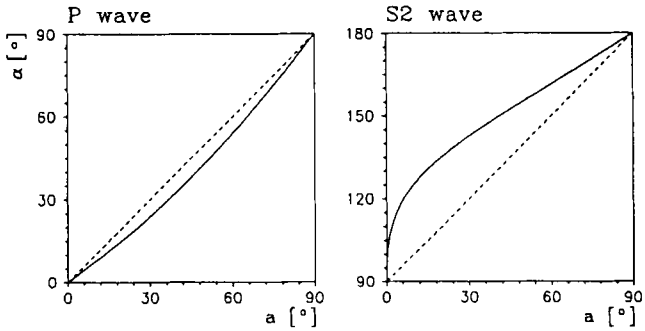

Figure 10. Polarization directions of the far-field P- and $S2$-waves. The polarization direction of P- and $S2$-waves as a function of receiver azimuth (full line) are displayed and compared with those for an isotropic medium (dashed line). The polarization direction is measured clockwise from the axis y.

The magnitude of anisotropy (see Fig. 9) is high as compared with medium models applicable in seismology. However, this medium serves as an example for illustrating anisotropy effects distinctly.

Radiation patterns

In this analysis the tensor m_{ij} was computed according to (7) and (9) for $f = 0.6$ Hz.

The radiation patterns of P- as well as S-waves (Fig. 11) are axially symmetric relative to the axes x, y; however, they are deformed in comparison with the isotropic medium (Fig. 4b). The form of the radiation pattern depends on the r/λ ratio, but the changes in radiation pattern are not only influenced by the near-field contributions, but also by the far-field waves, the amplitudes of which decrease with distance in different directions to a different degree. Analogously, as in an isotropic medium there are no directions, into which the source in the x–y plane would not radiate. Let us finally add that for P-waves in the x–y plane for $a = 0°$ and $r/\lambda = 0.5$ the near-field contributions are much more pronounced, compared with the isotropic medium.

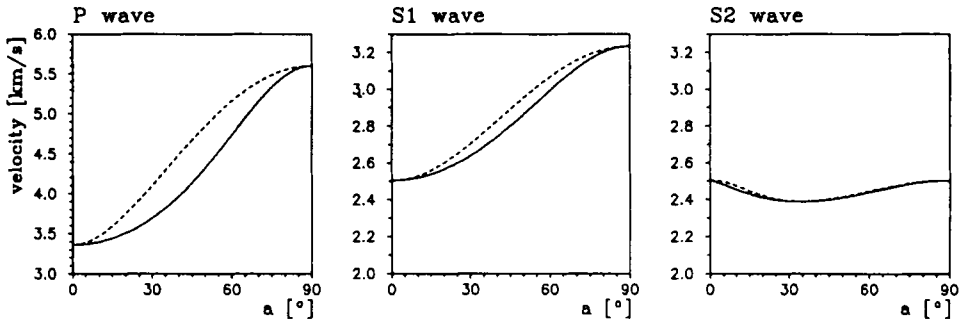

Figure 9. Phase and group velocity variations. The phase velocity as a function of the angle between the rotation symmetry axis and the slowness vector (dashed line) and the group velocity as a function between the rotation symmetry axis and the ray direction (full line) are shown for P-, $S1$- and $S2$-waves. For the given configuration the angle between the symmetry axis and the ray coincides with the receiver azimuth.

Downloaded from http://gji.oxfordjournals.org/ at Astronomical Institute CAS on August 4, 2015

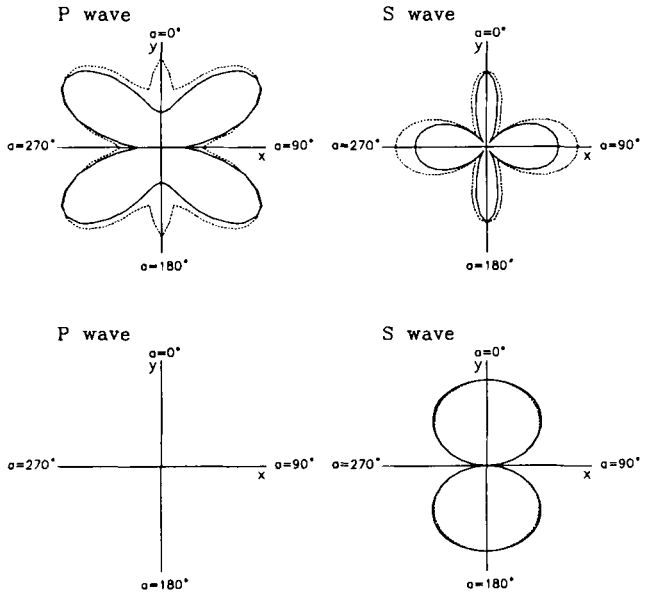

Figure 11. Radiation patterns of *P*- and *S*-waves excited by a line source situated in an anisotropic medium. The radiation patterns of *P*- and *S*-waves are shown in the x–y plane for component $v = [\dot{u}_x^2 + \dot{u}_y^2]^{1/2}$ (upper parts) and for component $w = |\dot{u}_z|$ (lower parts). The radiation patterns are measured at distances $r_1 = 4.7$ km [dotted line, $(r/\lambda_P)_{\min} = 0.5$, $(r/\lambda_S)_{\min} = 0.9$] and $r_2 = 9.3$ km [full line, $(r/\lambda_P)_{\min} = 1.0$, $(r/\lambda_S)_{\min} = 1.7$]. The radiation patterns are normalized to their maximum amplitude. The FD parameters used are: $\Delta x = \Delta y = 0.0910$ km, $\Delta t = 0.0075$ s, size of the model $330\,\Delta x \cdot 330\,\Delta y$, number of time levels $n = 800$.

Polarization

In order to study the polarization properties of waves, we will use the double-couple source (formulae 8, 9) for $f = 0.6$ Hz. This source generates *P*- and *S*2-waves only.

Polarization exhibits similar effects as in the case of an isotropic medium. *P*- and *S*2-waves are quasi-elliptically polarized and their ellipticity depends on receiver azimuth a and ratio r/λ. We can observe singularities in ellipticity for the far-field nodal-line directions and, in general, the decrease of ellipticity with increasing value of r/λ (see Figs 12, 13a and Table 2).

However, we have found some anomalies not detected in the isotropic medium:

(1) The decrease of ellipticity with increasing r/λ is strongly azimuthally dependent. For instance, in the azimuth interval of 6–18° and in the r/λ interval of 1.1–3.5 practically no decrease of ellipticity was observed for the *S*2-wave (see Fig. 13b).

(2) Fig. 13(b) shows, moreover, that in the vicinity of the source the predominant polarization direction of the complete waves can significantly deviate from the theoretical polarization direction of the far-field waves. As opposed to the *P*-wave, for which no clear difference in polarization direction has been found, for the *S*2-wave the difference is nearly $\Delta\alpha = 25°$ (see Fig. 14). Fig. 14 also shows that the difference $\Delta\alpha$ is a function of the r/λ ratio as well as of azimuth a. Let us add that the measurement of the difference $\Delta\alpha$ could not be performed for the whole azimuth interval. We had to confine ourselves to studying this effect for azimuths, for which the degree of ellipticity allowed the predominant polarization direction to be measured reliably (ellipticity $e < 50$ per cent).

5 CONCLUSIONS

The numerical modelling of complete wavefields in homogeneous isotropic and anisotropic media has led the author to the following conclusions:

(1) The radiation patterns of *P*- and *S*-waves of a point or a line double-couple source, situated in isotropic as well as in anisotropic media, have no nodal lines, i.e. for the exact solution of the wavefield there are no directions into which the source (point as well as line source) would not radiate energy.

(2) The *P*- and *S*-waves excited by a point double-couple source situated in a homogeneous isotropic medium, and the *P*- and *S*-waves excited by a line double-couple source situated in an anisotropic medium, do not have linear but quasi-elliptical polarization. The cause of 'ellipticity' is the presence of the near-field waves. The degree of ellipticity depends generally on the direction of the ray coming from the source and on the r/λ ratio. At the same time, the greatest contribution by the near-field waves is in the vicinity of the far-field nodal lines.

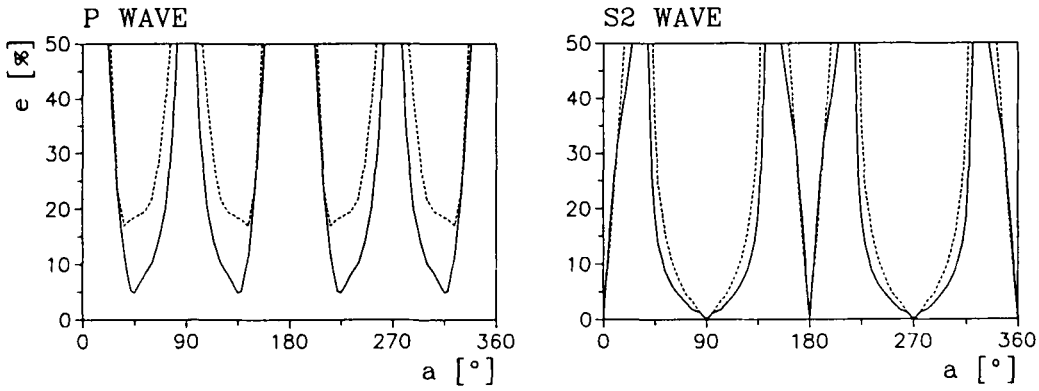

Figure 12. Ellipticity of waves excited by a line source as a function of the receiver azimuth. The ellipticity of *P*- and *S*-waves is measured at distances $r_1 = 4.7$ km [dotted line, $(r/\lambda_P)_{\min} = 0.5$, $(r/\lambda_S)_{\min} = 0.9$] and $r_2 = 9.3$ km [full line, $(r/\lambda_P)_{\min} = 1.0$, $(r/\lambda_S)_{\min} = 1.7$].

Downloaded from http://gji.oxfordjournals.org/ at Astronomical Institute CAS on August 4, 2015

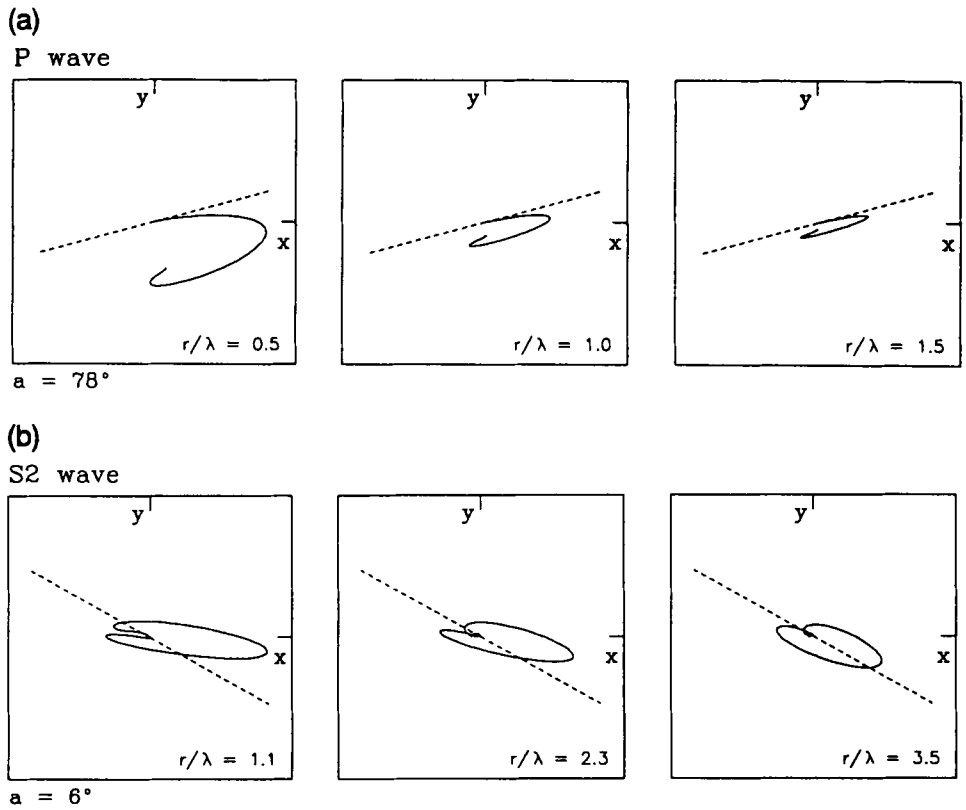

Figure 13. (a) Polarization diagrams of velocity records of *P*-waves excited by a line double-couple source situated in an anisotropic medium. For the receivers with azimuth $a = 78°$ at distances $r_1 = 4.7$ km ($r/\lambda = 0.5$), $r_2 = 9.3$ km ($r/\lambda = 1.0$) and $r_3 = 14.0$ km ($r/\lambda = 1.5$) from the source the polarization diagrams are shown (full line) and compared with the theoretical far-field polarization directions (dashed line, $\alpha = 75.1°$). (b) Polarization diagrams of velocity records of *S*2-waves excited by a line double-couple source situated in an anisotropic medium. For the receivers with azimuth $a = 6°$ at distances $r_1 = 4.7$ km ($r/\lambda = 1.1$), $r_2 = 9.3$ km ($r/\lambda = 2.3$) and $r_3 = 14.0$ km ($r/\lambda = 3.5$) from the source the polarization diagrams are shown (full line) and compared with the theoretical far-field polarization directions (dashed line, $\alpha = 119.5°$).

Table 2. Contamination of waves by the near-field contributions—anisotropic medium.

P wave		S wave	
$(r/\lambda)_{min}$	c[%]	$(r/\lambda)_{min}$	c[%]
0.5	76	1.1	44
1.0	54	2.3	39

c denotes the interval width (in per cent) of directions in which a 'significantly contaminated far-field wave' is radiated.

(3) For a point as well as a line double-couple source situated in a homogeneous isotropic medium and ratio $r/\lambda = 9$, the polarization of the radiated wave is significantly influenced by the near-field contributions (ellipticity $e > 20$ per cent) in a direction interval, which amounts to almost 10 per cent of the whole interval of angles.

(4) For a line double-couple source situated in an anisotropic medium, a difference between the predominant polarization direction of the complete waves and the theoretical far-field polarization directions was observed. The difference for the *S*2-wave is $\Delta\alpha = 25°$ for $a = 6°$ and $r/\lambda = 1.1$. The deviation decreases with increasing r/λ and is azimuthally dependent.

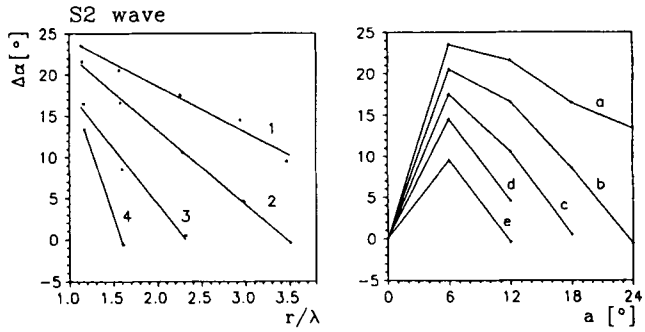

Figure 14. Difference $\Delta\alpha$ between the *S*2-wave predominant polarization direction and the theoretical far-field polarization directions as a function of ratio r/λ and azimuth a. The difference $\Delta\alpha$ is depicted as a function of ratio r/λ for azimuths $a = 6°$ (line 1), $a = 12°$ (line 2), $a = 18°$ (line 3) and $a = 24°$ (line 4), and as a function of azimuth a at distances $r_1 = 4.7$ km (line a, $r/\lambda = 1.1$), $r_2 = 6.4$ km (line b, $r/\lambda = 1.6$), $r_3 = 9.3$ km (line c, $r/\lambda = 2.3$), $r_4 = 12.1$ km (line d, $r/\lambda = 2.9$) and $r_5 = 14.0$ km (line e, $r/\lambda = 3.5$).

ACKNOWLEDGMENTS

I would like to thank Ivan Pšenčík and Jiří Zahradník for many discussions on the subject.

Downloaded from http://gji.oxfordjournals.org/ at Astronomical Institute CAS on August 4, 2015

REFERENCES

Aboudi, J., 1971. Numerical simulations of seismic sources, *Geophysics*, **36**, 810–821.

Aki, K. & Richards, P. G., 1980. *Quantitative Seismology, Theory and Methods I, II*, W. H. Freeman, San Francisco.

Alford, R. M., Kelly, K. R. & Boore, D. M., 1974. Accuracy of finite-difference modelling of the acoustic wave equation, *Geophysics*, **39**, 834–842.

Alterman, Z. & Loewenthal, D., 1970. Computer generated seismograms, in *Methods in Computational Physics*, vol. 12, pp. 35–164, ed. Bolt, B. A., Academic Press, New York.

Crampin, S., Stephen, R. A. & McGonigle, R., 1982. The polarization of *P*-waves in anisotropic media, *Geophys. J.R. astr. Soc.*, **68**, 477–485.

Červený, V., Molotkov, I. A. & Pšenčík, I., 1977. *Ray Methods in Seismology*, Charles University Press, Prague.

Daudt, C. R., Braile, L. W., Nowack, R. L. & Chiang, C. S., 1989. A comparison of finite-difference and Fourier method calculations of synthetic seismograms, *Bull. seism. Soc. Am.*, **79**, 1210–1230.

Farra, V., Bernard, P. & Madariaga, R., 1986. Fast near source evaluation of strong ground motion for couple source modes, in *Earthquake Source Mechanisms*, Geophysical Monographs, vol. 37, pp. 121–130, AGU 1986.

Frankel, A. & Clayton, R. W., 1986. Finite difference simulations of seismic scattering: Implications for the propagation of short-period seismic waves in the crust and models of crustal heterogeneity, *J. geophys. Res.*, **91**, 6465–6489.

Fryer, G. J. & Frazer, L. N., 1984. Seismic waves in stratified anisotropic media, *Geophys. J.R. astr. Soc.*, **78**, 691–710.

Gajewski, D. & Pšenčík, I., 1987. Computation of high-frequency seismic wavefields in 3-D laterally inhomogeneous anisotropic media, *Geophys. J.R. astr. Soc.*, **91**, 383–411.

Gajewski, D. & Pšenčík, I., 1990. Vertical seismic profile synthetics by dynamic ray tracing in laterally varying layered anisotropic structures, *J. geophys. Res.*, **95**, 11 301–11 315.

Hong, M. & Bond, L. J., 1986. Application of finite difference method in seismic source and wave diffraction simulation, *Geophys. J.R. astr. Soc.*, **87**, 731–752.

Keith, C. M. & Crampin, S., 1977. Seismic body waves in anisotropic media: synthetic seismograms, *Geophys. J.R. astr. Soc.*, **49**, 225–243.

Kelly, K. R., Ward, R. W., Treitel, S. & Alford, R. M., 1976. Synthetic seismograms: a finite-difference approach, *Geophysics*, **41**, 2–27.

Levander, A. R., 1988. Fourth-order finite-difference *P-SV* seismograms, *Geophysics*, **53**, 1425–1436.

Mallick, S. & Frazer, L. N., 1990. Computation of synthetic seismograms for stratified azimuthally anisotropic media, *J. geophys. Res.*, **95**, 8513–8526.

Mandal, B. & Mitchell, B. J., 1986. Complete seismogram synthesis for transversely isotropic media, *J. Geophys.*, **59**, 149–156.

Mandal, B. & Toksöz, M. N., 1990. Computation of complete waveforms in general anisotropic media — results from an explosion source in an anisotropic medium, *Geophys. J. Int.*, **103**, 33–45.

Mitchell, A. R., 1969. *Computational Methods in Partial Differential Equations*, John Wiley & Sons, New York.

Taylor, D. B., 1987. Double contour integration for transmissions from point sources through anisotropic layers as used in ROCPAC software, *Geophys. J.R. astr. Soc.*, **91**, 373–381.

Tsingas, C., Vafidis, A. & Kanasewich, E. R., 1990. Elastic wave propagation in transversely isotropic media using finite differences, *Geophys. Prosp.*, **38**, 933–949.

Tsvankin, I. D. & Chesnokov, E. M., 1990. Synthesis of body wave seismograms from point sources in anisotropic media, *J. geophys. Res.*, **95**, 11 317–11 331.

Downloaded from http://gji.oxfordjournals.org/ at Astronomical Institue CAS on August 4, 2015